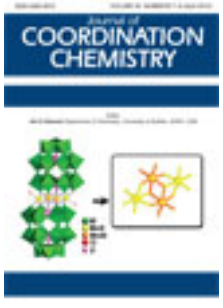

Journal of Coordination Chemistry
Publication details, including instructions for authors and subscription information:
http://www.tandfonline.com/loi/gcoo20

Syntheses and characterization of new tetraazamacrocyclic copper(II) complexes as a dual functional mimic enzyme (catalase and superoxide dismutase)

Abd El-Motaleb M. Ramadan [a]
[a] Chemistry Department, Faculty of Science , Kafr El-Sheikh University , Kafr El-Sheikh 33516 , Egypt
Published online: 30 Mar 2012.

To cite this article: Abd El-Motaleb M. Ramadan (2012) Syntheses and characterization of new tetraazamacrocyclic copper(II) complexes as a dual functional mimic enzyme (catalase and superoxide dismutase), Journal of Coordination Chemistry, 65:8, 1417-1433, DOI: 10.1080/00958972.2012.673719

To link to this article: http://dx.doi.org/10.1080/00958972.2012.673719

Journal of Coordination Chemistry
Vol. 65, No. 8, 20 April 2012, 1417–1433

Taylor & Francis
Taylor & Francis Group

Syntheses and characterization of new tetraazamacrocyclic copper(II) complexes as a dual functional mimic enzyme (catalase and superoxide dismutase)

ABD EL-MOTALEB M. RAMADAN*

Chemistry Department, Faculty of Science, Kafr El-Sheikh University, Kafr El-Sheikh 33516, Egypt

(*Received 14 September 2011; in final form 10 February 2012*)

A series of macrocyclic complexes, $[Cu(TAAP)]X_2$, $X = ClO_4$ and CH_3COO; [Cu(TAAP)X]X, $X = NO_3$, Cl, and Br, have been synthesized by self-condensation of 5-amino-3-methyl-l-phenylpyrazole-4-carbaldehyde (AMPC) in the presence of copper(II). Elemental analyses and conductivity measurements confirm the stoichiometry of the ligand and complexes, while the characteristic absorption bands in IR spectra confirmed the formation of ligand framework around copper. Square-pyramidal and square-planar stereochemistries have been proposed for the five-coordinate (nitrato and halogeno) and four-coordinate (perchlorate and acetate) complexes. The electrochemical properties and thermal behaviors have been studied by cyclic voltammetry and TGA. Mimetics of antioxidant enzymes such as superoxide dismutase (SOD) and catalase demonstrated that there is a correlation between the observed redox properties and the SOD and catalase biomimetic catalytic activities of the copper(II) complexes.

Keywords: Synthesis; SOD; Copper(II); Catalase; Biomimetic; Catalytic activity

1. Introduction

Superoxide anion radical ($O_2^{\cdot-}$) generated by a number of enzymes in the course of their reaction cycle, with production of superoxide anion and reactive oxygen species (ROS) derived from it, is the respiratory chain within mitochondria [1]. Approximately 0.4–4% of oxygen consumed during normal respiration is converted to superoxide anion radical ($O_2^{\cdot-}$) within the mitochondria [2–4]. The brain, which accounts for about 20% of the total oxygen consumption in humans, while comprising only 2% of body weight, is particularly vulnerable to oxidative stress [5]. Another particularly vulnerable organ, due to its high oxygen consumption, is the heart. Vast literature supports the deleterious roles of ROS in a broad array of diseases including autoimmune, inflammatory disorders such as rheumatoid arthritis (RA) and ischemic diseases as well as organ failure from species or trauma [6]. There is much evidence implicating oxidative stress and mitochondrial dysfunction in Alzheimer's and Parkinson's diseases, amyotrophic

*Email: ramadanss@hotmail.com

ISSN 0095-8972 print/ISSN 1029-0389 online
http://dx.doi.org/10.1080/00958972.2012.673719

lateral sclerosis, Friedreich Ataxia, prion disease and, indeed, in aging and age-associated decline [7]. Combination of $O_2^{\cdot-}$, to NO yields peroxynitrite ($ONOO^-$), a cytotoxic, tissue-damaging agent that oxidizes protein residues [6]. Peroxynitrite ($ONOO^-$) has been implicated with a major role in oxidative stress in a number of diseases including RA, inflammatory bowel disease, atherosclerosis, and pulmonary diseases [6]. Key cellular antioxidant enzymes which can lower the level of ROS e.g., $O_2^{\cdot-}$, H_2O_2, $HO^{\cdot}$, and $ONOO^-$ are the antioxidant metalloproteinases, such as SODs, catalase, and peroxidase. Numerous studies have indicated that these antioxidant compounds are therapeutic agents for a variety of disorders associated with oxidative stress. However, SODs have molecular weight too high to cross cell membranes and can only provide intracellular protection [8]. Also, its short half-life (<30 min) observed after intravenous administration limits its therapeutic utility [8]. The main problems in use of SOD as a drug are the nonhuman origin of the enzyme and its rapid metabolism in human body. SOD, a rather protein, may be antigenic and including anaphylactic shock. In order to circumvent these difficulties, low-molecular mass transition metal complexes that mimic the enzyme activity have been investigated. Mimetics of antioxidant enzymes such as SODs or catalases are presented as potential new drugs to prevent oxidative stress damage [9]. Diseases that may be treatable with SOD mimics include heart attack, stroke, autoimmune diseases (such as osteoarthritis), neurodegenerative diseases (including Alzheimer's and Parkinson's), and aging. A totally selective catalyst for eliminating $O_2^{\cdot-}$, the production of pro-inflammatory cytokines can also be eliminated. The relative advantages of a selective SOD mimetic and a multifunctional scavenger for therapeutic use have been debated, with one cited advantage being that a selective SOD mimetic could be used to probe the role of superoxide in disease [6]. However, there is good reason to believe that added activity against other reactive species, in particular hydrogen peroxide and peroxynitrite, would confer significant therapeutic advantage. SOD activity alone can decrease peroxynitrite through removing one of its components, superoxide. However, the SOD reaction produces hydrogen peroxide, implying that in some circumstances SOD alone might enhance toxicity. For example, whereas Mn–Salens, a class of synthetic SOD/catalase mimetics, protected brain slices from anoxia/reoxygenation, bovine SOD potentiated the injury [10]. Similarly, Mn–Salens protected an intestinal cell model against oxidative injury during lactic acidosis, while bovine SOD exacerbated injury unless administered in combination with bovine liver catalase [10, 11]. Baker *et al*. [12] carried out an evaluation of the effectiveness of Mn–Salens in a rat focal ischemia model involving middle cerebral artery occlusion. Overall, this study suggested that synthetic SOD/catalase mimetics might serve as multifunctional therapeutic agents for stroke [12]. Such observations suggest that compounds exhibiting both SOD and catalase activities, along with the ability to scavenge RNS, should have distinct, qualitative advantages over those having only SOD activity. These include not only the potential to inactivate numerous damaging species but also the reduced likelihood of exacerbating injury through generation of hydrogen peroxide. These therapeutic benefits of SOD/catalase mimics as well as the lack of clinical success with proteins of these antioxidants have fueled efforts to develop metal coordination complexes as SOD/catalase mimics and most of them appear to be efficient [6, 9, 12, 13]. The problem is that they lose their antioxidant mimetic catalytic activity *in vivo* [14, 15]. Proteins appeared to have better affinities than the studied ligands for $M^{(n+)}$ center, which is inactivated once it is imbedded in the proteins.

Thus, $M^{(n+)}$ must be enclosed in a stable ligand system, which protects it from being chelated by serum and cellular components. However, the balance between sufficient stability necessary to survive *in vivo* conditions and certain flexibility that allows change of metal coordination occurring during the catalytic process is a substantial requirement. Additionally, the ligand system must allow $M^{(n+)}$ redox center to dismutate $O_2^{\cdot-}$. In order to meet these requirements, it has been suggested that macrocyclic ligand enhances complex stability and may have higher biological stability [16–18].

As a part of our studies on chemical and biological properties of metal complexes, we present here detailed template synthesis and spectroscopic characterization of new tetraazamacrocyclic copper(II) complexes as dual functional antioxidant (SOD/catalase) enzymes to elucidate the structure reactivity relationship. Cyclic voltammetry measurements are performed to correlate the redox properties of these macrocyclic copper(II) complexes with their SOD/catalase biomimetic catalytic activities.

2. Experimental

2.1. *Materials*

All chemicals were of analytical grade. 5-Amino-3-methyl-l-phenylpyrazole-4-carbaldehyde (AMPC) was prepared according to the method described elsewhere [19].

2.2. *Synthesis of the tetraazamacrocyclic copper(II) complexes*

A solution of freshly prepared AMPC (0.024 mol) in absolute ethanol (50 mL) was heated and stirred. While the AMPC solution was under reflux, a solution of the appropriate amount of copper(II) salt in 50 mL of absolute ethanol was added. The reaction mixture was boiled under reflux and stirred for 8 h, during which colored products precipitated. After cooling, the solution was filtered and the isolated solid was washed with ethanol and ether and finally dried *in vacuum* over CaO at room temperature for 2 weeks.

2.3. *Physical measurements*

Infrared (IR) spectra were recorded using KBr pellets from 4000 to 200 cm^{-1} on a Unicam SP200 spectrophotometer. Electronic absorption spectra were obtained in DMF solution with a Shimadzu UV-240 spectrophotometer. Magnetic moments were measured by Gouy's method at room temperature. ESR measurements of polycrystalline samples at room temperature were made on a Varian E9 X-band spectrometer using a quartz Dewar vessel. All spectra were calibrated with DPPH ($g = 2.0027$). The specific conductances of the complexes were measured using freshly prepared 10^{-3} mol L^{-1} solutions in electrochemically pure MeOH or DMF at room temperature, using an YSI Model 32 conductance meter. Thermogravimetric measurements were performed using a Shimadzu TG 50-Thermogravimetric analyzer from 25°C to 800°C under N_2. Elemental analyses (C, H, and N) were carried out at the Microanalytical Unit of Cairo University.

2.4. *Electrochemical measurements*

Cyclic voltammetric measurements were performed by a computerized Electrochemical Trace Analyzer Model 273 A-PAR (Princeton Applied Research, Oak Ridge, TN, USA) controlled *via* 270/250 PAR software. The electrode assembly (Model 303 A-PAR) incorporating a micro-electrolysis cell of a three electrode system, comprising a hanging mercury drop electrode as a working electrode (area: $0.026\,cm^{-1}$), a $Ag/AgCl/KCl_s$ reference electrode and a platinum wire counter electrode, was used. Stirring of the solution in the micro-electrolysis cell was performed using a magnetic stirrer (305-PAR) to provide convective transport during the pre-concentration step. The measurements were automated and controlled through the programming capacity of the apparatus. The supporting electrolyte was $0.1\,mol\,L^{-1}$ n-Bu_4NClO_4. The solvents used were pure and the concentration of the complexes was $0.001\,mol\,L^{-1}$.

2.5. *SOD assays*

SOD mimetic catalytic activity of the copper(II) complexes was assayed by using phenazine methosulphate (PMS) to photogenerate a reproducible and constant flux of $O_2^{\cdot-}$ at pH = 8.3 (phosphate buffer). Reduction of nitroblue tetrazolium (NBT) to blue formazan was used as an indicator of $O_2^{\cdot-}$ production and followed spectrophotometrically at 560 nm. The addition of PMS ($9.3 \times 10^{-5}\,mol\,L^{-1}$), to NBT ($1.7 \times 10^{-4}\,mol\,L^{-1}$) and phosphate buffer (final volume of 2 mL) caused an $OD(\Delta_1)_{560}\,min^{-1}$ change of 0.035. Reaction blank samples and in the presence of copper(II) complexes were measured for 5 min.

2.6. *Catalase-like activity assays*

Catalase-like activity of the copper(II) models was assessed by measuring the rate constant k_{obs} for catalytic decomposition of H_2O_2. The course of the reaction was followed spectrophotometrically by monitoring decreases in the characteristic absorbance of [catalyst-H_2O_2] adduct at 385 nm. A 1 mL solution of the copper(II) complexes ($0.002\,mol\,L^{-1}$) and 1 mL solution of H_2O_2 ($0.02\,mol\,L^{-1}$) were combined in a quartz cell at room temperature in the presence of 1 mL of phosphate buffer pH = 7 ($0.1\,mol\,L^{-1}$). The absorbance changes at 385 nm were recorded at different time intervals. The effect of varying the amount of both catalyst and H_2O_2 was studied.

3. Results and discussion

Self-condensation of AMPC in the presence of copper(II) yields a new series of macrocyclic cationic complexes, $[Cu(TAAP)]X_2$, $X = ClO_4$ and CH_3COO; [Cu(TAAP)X]X, $X = NO_3$, Cl, and Br (scheme 1), containing self-condensed AMPC. The self-condensation of AMPC under the influence of metal ions requires that the condensation be initiated several minutes before the metal ion is added. This provides adequate opportunity for prior formation of the free tetramer, which may then rearrange under the influence of metal ion. Formation of the fully cyclized ligand

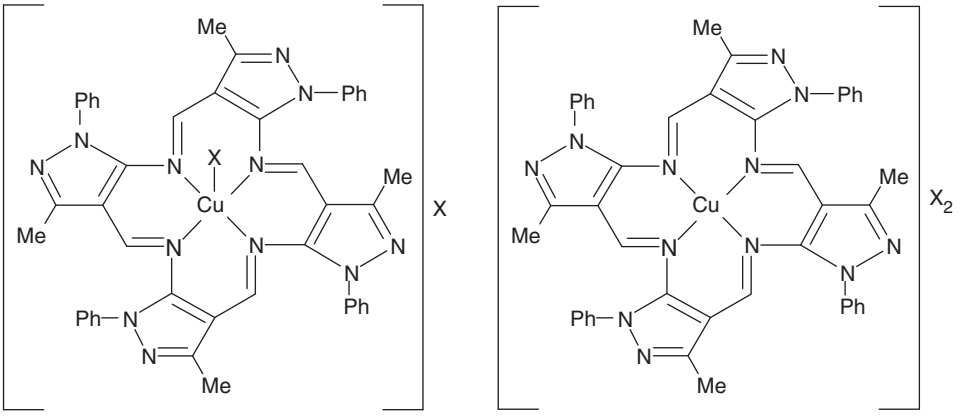

Complex **1**, X = Cl; **2**, X = Br; **3**, X = NO_3 Complex **4**, X = AcO; **5**, X = ClO_4

Scheme 1. Structure of copper(II) tetraazamacrocyclic complexes **1**–**5**.

Table 1. Molecular formulae, elemental analyses, and physical properties of the tetraazamacrocyclic copper(II) complexes.

			Found (Calcd)			
Complex	Color	Λ ($\Omega^{-1}\,cm^2\,mol^{-1}$)	C	H	N	M
1	Orange	81.80	60.77(60.92)	4.13(4.15)	19.22(19.39)	7.82(7.33)
2	Brownish yellow	75.16	55.33(55.26)	3.67(3.77)	17.44(17.59)	6.93(6.65)
3	Dark brown	77.96	52.21(52.29)	4.45(4.55)	16.65(16.55)	6.32(6.29)
4	Pale brown	145.78	62.97(63.04)	4.37(4.59)	18.11(18.40)	7.23(6.95)
5	Dark red	148.65	53.12(53.08)	3.57(3.62)	16.86(16.90	6.39(6.77)

framework and the complexes was deduced on the basis of elemental analyses and thermal investigations (TGA and DTG) in addition to spectral, electrochemical, and magnetic measurements. The elemental analyses (table 1) agree well with the proposed structure of the tetraazamacrocyclic Schiff-base copper(II) complexes. The molar conductivity data for *ca* $10^{-3}\,mol\,L^{-1}$ of [Cu(TAAP)X]X, X = NO_3, Cl, and Br, in DMF solutions at room temperature are in accord with those expected for a 1:1 electrolyte, while the measured values for [Cu(TAAP)]X_2, X = ClO_4 and CH_3COO, under the same conditions are as expected for a 2:1 electrolyte. These observations imply that one of the anions in [Cu(TAAP)X]X is coordinated to copper(II), while the perchlorate and the acetate in [Cu(TAAP)]X_2 solution do not participate in coordination. The pure isolated complexes are microcrystalline, stable in atmosphere, and soluble in most polar organic solvents.

3.1. *IR spectra*

Preliminary identification of the complexes was obtained from IR spectra. The absence of the characteristic stretching and deformation frequencies expected for $\nu(NH_2)$ and

C=O of free AMPC suggests that complete self-condensation of the amino and the carbonyl have taken place. The observed strong intensity band at 1590–1600 cm^{-1} characteristic of ν(C=N) provides strong evidence for the presence of cyclic product [20]. The ν(C=N) of the synthesized complexes is lower than the expected value. This lower value of ν(C=N) may be explained on the basis of lone pair density of azomethine nitrogen shifting to copper [21, 22], indicating that coordination takes place through nitrogen of C=N. Formation of the macrocyclic framework has further been deduced by appearance of a medium intensity band at 440–460 cm^{-1}, assignable to ν(M–N) [23]. Spectra of the copper(II) complexes are similar to spectra of the structurally analogous $[Pd(TAAP)]^{2+}$, $[Pd(TAAP)]^{2+}$ [24], and $[Ni(TAAB)]^{2+}$ [25]. Bands attributed to functional groups in the macrocycles are observed in the following regions (cm^{-1}): 3000–3150, aromatic ν(C–H), 2900–3000; aliphatic ν(C–H), 1610–1620; ν(C=C), 1560–1575 and the out of plane bending of phenyl, at *ca* 710–745.

The IR absorptions of the anions in these complexes show that perchlorate and acetate are not coordinated [26]. This finding was inferred from strong broad bands at 1085 and 621 cm^{-1} and a medium broad band at 412 cm^{-1} for perchlorate and at 1680, 1258, and 412 cm^{-1} for acetate. The spectrum of the nitrato complex exhibits vibration modes of nitrate assignable for ν(M–O) of unidentate ONO_2. The asymmetric stretching frequency for nitrate ν_3 occurs as a strong absorption at 1390 cm^{-1} [26]. The weak band at 725 cm^{-1} may be assigned to ν_2 of nitrate. These spectral features suggest that this complex contains both coordinated monodentate nitrate and free nitrate [27]. Absorptions due to lattice water are evident in the spectrum of nitrate complex, occurring as a broad absorption at 3400 cm^{-1} and a weak shoulder at 1650 cm^{-1} [26]. For halogeno complexes ([CuL(TAAP)]X; X = Cl or Br), the nonelectrolyte halogen exhibits far IR absorptions at 310–340 cm^{-1}, indicating an apical coordinated halide [26].

3.2. *Electronic absorption spectra*

Electronic spectra of the copper(II) macrocyclic complexes in DMF solutions at room temperature are tabulated in table 2. In square-pyramidal copper(II) complexes the d-orbital energy level scheme (idealized symmetry group C_{4v}) is $d_{x^2-y^2} > d_{z^2} > d_{xy} > d_{xz}$, d_{yz}. Accordingly, electronic spectra of the five-coordinate copper(II) complexes

Table 2. Electronic absorption spectra (cm^{-1}) of copper(II) complexes **1–5**.

	λ_{max} (nm)		
Complex	$^2B_{1g} \rightarrow {}^2B_{2g}$	$^2B_{1g} \rightarrow {}^2A_{1g}$	$^2B_{1g} \rightarrow {}^2E_g$
4	716	600	510
5	700	595	500
	$d_{xz}\ d_{yz} \rightarrow d_{x^2-y^2}$	$d_{xy} \rightarrow d_{x^2-y^2}$	
1	515	610	
2	520	617	
3	505	630	

Complex details are as listed in table 1.

in square-pyramidal geometry show three d–d bands [28], assigned to the transitions $d_{z^2} \rightarrow d_{x^2-y^2}$, $d_{xy} \rightarrow d_{x^2-y^2}$, and d_{xz}, $d_{yz} \rightarrow d_{x^2-y^2}$. The energy level sequence depends on the amount of distortion due to the ligand field and the Jahn–Teller effect [28]. The electronic spectra of the halide and nitrate complexes reported here show two bands at 610–630 and 505–520 nm, assigned to the d_{xz}, $d_{yz} \rightarrow d_{x^2-y^2}$ and $d_{xy} \rightarrow d_{x^2-y^2}$ transitions, respectively. Because of the low intensity of $d_{z^2} \rightarrow d_{x^2-y^2}$ transition, this band is usually not observed as a separate band in tetragonally distorted complexes.

The electronic absorption spectra of the four-coordinate perchlorate and acetate complexes display three d–d transitions at 700–716, 595–600, and 500–510 nm, assignable to $^2B_{1g} \rightarrow {}^2B_{2g}$, $^2B_{1g} \rightarrow {}^2A_{2g}$, and $^2B_{1g} \rightarrow {}^2E_{2g}$, respectively [28]. The geometries of the copper(II) tetraazamacrocyclic complexes is supported by magnetic measurements.

3.3. *ESR spectra and magnetic moment studies*

The room temperature magnetic moments and details of the polycrystalline ESR spectra of the copper(II) complexes are listed in table 3. The data in table 3 display magnetic moments in the 1.82–2.05 BM range, corresponding to one unpaired electron [29] and consistence with monomeric complexes [29]. These normal magnetic moments exclude significant interaction between neighboring copper(II) ions in the polycrystalline state [29], further confirmed from ESR spectra.

ESR spectra of the copper(II) complexes were recorded as polycrystalline samples on X-band at 9.1 GHz under the magnetic field strength 3100 *G*, scan rate 1000, and recorded at room temperature. The $g_{||}$ and $g_{\perp}$ values were computed from the spectrum using DPPH free radical as "*g*" marker. In square-planar geometry the unpaired electron lies in the $d_{x^2-y^2}$ orbital giving $^2B_{1g}$ as the ground state with $g_{||} > g_{\perp}$. The observed *g* values of both perchlorate and acetate complexes (table 3) are characteristics of square-planar geometry. Kivelson and Neiman [30] reported the $g_{||} < 2.3$ for covalent metal ligand bond and $g_{||} > 2.3$ for ionic character. The trend $g_{||} > g_{\perp} > g_e$ (2.0023) observed for these complexes show that the unpaired electron is localized in the $d_{x^2-y^2}$ orbital of copper(II). The *g* values are related by the expression $G = (g_{||} - 2)/(g_{\perp} - 2)$ which measures the exchange interaction between copper centers in the polycrystalline solid. The *G* values 4.489–4.535 exclude any exchange interaction between the copper(II) centers.

Table 3. Magnetic moment values and ESR spectral data of copper(II) complexes **1–5**.

Complex	g_1	g_2	g_3	R	μ_{eff} (BM)
1	2.336	2.190	2.092	0.6712	2.03
2	2.503	2.289	2.129	0.7477	1.98
3	2.261	2.204	2.161	0.7544	1.88
	$g_{||}$	$g_{\perp}$	g_{av}	G	
4	2.409	2.041	2.197	4.489	1.82
5	2.449	2.099	2.216	4.535	1.95

Complex details are as listed in table 1.

For five-coordinate halogeno and nitrato complexes, square-pyramidal or trigonal-bipyramidal must be considered. The spectral features of these complexes are similar and exhibit intense ESR signals that are characteristic of the rhombic symmetry with three g-values. The three observed g-values (g_1, g_2, and g_3 in order of decreasing magnitude) were computed from the spectra. Square-pyramidal and trigonal-bipyramidal are characterized by $d_{x^2-y^2}$ and d_{z^2} the ground states, respectively [28]. For systems with $g_3 > g_2 > g_1$ the ratio of $(g_2 - g_1)/(g_3 - g_2) = R$ is useful to distinguish geometry. If the ground state is d_{z^2} the value of R is greater than 1; for ground state predominantly $d_{x^2-y^2}$ the value of R is less than 1. The three complexes under study show values of R (table 3) less than 1, and these results confirm five-coordinate, square-pyramidal geometry.

3.4. *Thermal studies*

The above results are confirmed by thermogravimetric studies. The TGA curves were obtained in N_2 from 75°C to 720°C. The decomposition stages, temperature ranges, maximum decomposition peaks DTG_{max}, percentage losses in mass, and the assignment of decomposition moieties are given in table 4.

The thermogravimetric curves of the acetate and halide complexes are similar and exhibit two stages of decomposition from ambient to 720°C. The initial weight loss is due to removal of the counter anions, at 170°C and ends at 250°C; the observed weight losses are in agreement with calculated values. Since decomposition started at 170°C the presence of any solvent/water may be ruled out. The sharp weight loss between 210°C and 720°C in TGA curve represents decomposition of the compounds into copper oxide. The total loss of weight agrees with calculated data.

For the macrocyclic nitrato complex thermal decomposition occurs in three stages from 75°C to 580°C. The first stage is dehydration from 75°C to 150°C, corresponding to five water molecules. The second decomposition from 150°C to 220°C (mass loss of 12.38%) is due to explosion of nitrates. The final degradation comprises several successive and unresolved steps from 220°C to 580°C, with maximum decomposition DTG_{max} at 500°C. The corresponding mass losses are due to complete decomposition with mass loss in agreement with calculated and the final product is CuO.

Table 4. Thermogravimetric analysis data of the tetraazamacrocyclic copper(II) complexes **1–4**.

Complex	Step	DTG (°C)	Temperature range (°C)	Mass loss (%) Found (Calcd)	Species formed
[CuLCl]Cl	1	180	170–210	08.89(08.19)	CuL
	2	410	210–500	14.54(14.78)	$CuL_{(0.825)}$
	3	635	500–720	67.95(68.43)	CuO
[CuLBr]Br	1	215	190–250	16.55(16.73)	CuL
	2	680	250–720	74.87(75.36)	CuO
$[CuL(NO_3)](NO_3)5H_2O$	1	110	75–150	08.69(08.91)	$[CuL(NO_3)](NO_3)$
	2	210	150–220	12.38(12.28)	CuL
	3	500	220–580	71.21(71.37)	CuO
$[CuL](AcO)_2$	1	200	190–225	12.59(12.91)	CuL
	2	500	225–600	78.12(78.75)	CuO

3.5. *Electrochemical properties*

In order to obtain a deeper insight into the origin of SOD and catalase biomimetic catalytic activity of the copper(II) complexes, their electrochemical behavior was examined by cyclic voltammetry in the potential range 0.0–1.5 V in dimethylformamide containing 10^{-1} mol L^{-1} tetra (*n*-butyl) ammonium perchlorate. The cyclic voltammogram of the chloro complex is provided in "Supplementary material." All the complexes undergo reduction and oxidation potentials in the positive potential range. The couples correspond to reversible one electron transfer.

The reductive cyclic voltammograms show a potential gap between the first one-electron transfer and the second process. The occurrence of two cathodic contributions on the first scan suggests that the first process corresponds to the formation of one-electron reduction product of copper ($Cu^{II} \rightarrow Cu^{I}$). The last peak could be attributed to reduction of the Schiff base linkages of the tetraazamacrocycle. Evidence of copper deposition on the electrode surface was not observed. On the reverse scan only one broad oxidation peak is observed which is assigned to $Cu^{I} \rightarrow Cu^{II}$. This redox behavior reflects that these complexes are stable enough for copper(II) and copper(I). Table 5 summarizes the half-wave potential (ΔE_p) data calculated as the arithmetic mean of E_{pc} and E_{pa}. The $E_{1/2}$ values lie between the potentials of the reduction of O_2 to $O_2^{\cdot-}$ at -0.14 V *versus* NHE at pH = 7 and $O_2^{\cdot-}$ to H_2O_2 at $+0.89$ V *versus* NHE at pH = 7 as expected for compounds with SOD-like activity in dependence on the $O_2^{\cdot-}$ concentration [31].

The template synthesized tetraazamacrocyclic ligand and its copper(II) complexes have an unsaturated N_4 macrocyclic cavity. Oxidation potential of the metal center is influenced by the axial anions, e.g., Cl, Br, or NO_3. The axial chloro and bromo complexes are oxidized at less positive potentials (except nitrato complex) than those of other complexes, due to the higher basicity of the halogeno donors than the other anions.

3.6. *SOD biomimetic catalytic activity*

Low molecular weight complexes as SOD functional models containing transition metal ions have been proposed [32] to overcome the limitations of the use for SOD enzymes as therapeutic agents and pharmaceutical tools [33]. A copper(II) complex to be considered to possess SOD-like activity must fulfill some requirements: (a) flexible arrangement of the ligands around copper(II) to allow facile reduction to copper(I), (b) stability to avoid dissociation in the acid region, (c) an accessible site for the $O_2^{\cdot-}$

Table 5. Electrochemical data (mv) and catalase-like activities of **1–5**.

Complex	E_{pc}	E_{pa}	$E_{1/2}$	ΔE_p	$k_{obs} \times 10^3$ (min^{-1})
1	348	282	315.0	66	20.85
2	420	355	387.5	65	18.70
3	320	262	291.0	60	28.33
4	447	385	416.0	62	07.83
5	430	365	397.5	65	10.42

Complex details are as listed in table 1.

radical and, hence, to give rapid reduction to copper(I), and (d) an equatorial field of medium strength because strong ones would not favor attack of $O_2^{\cdot-}$ to the accessible apical sites. The spectral and electrochemical investigations demonstrated that the macrocyclic system provides these requirements for its copper(II) complexes as SOD functional models. Macrocycles and their metal complexes have been suggested as promising agents for diagnosis and treatment of different diseases [34] and as a potential class of SOD mimics, mainly because of their high thermodynamic stability [35].

SOD mimetic activity of the copper(II) complexes were assayed by using PMS as a photogenerator of the superoxide anion radical in association with NBT chloride as scavenger of the generated superoxide [36]. Inhibition of the reduction of NBT to formazan (F) by the synthesized copper(II) complexes was used for detection of SOD-like activity in phosphate buffer under similar biological conditions as previously described [27]. Inhibition of NBT is followed spectrophotometrically in the presence of various amounts of the copper(II) complexes. The IC_{50} concentrations can be obtained from the percentage inhibition (% NBT inhibition) of NBT ($\Delta A_o \times 100/\Delta A_o - \Delta A$) *versus* complex concentration plots. The percentage inhibition (% NBT inhibition) of NBT was calculated from the following equation: % NBT inhibition $= (\Delta A_c/\Delta A_c - \Delta A_s) \times 100$, where ΔA_o is the change in absorbance of the control containing the reaction mixture at 560 nm in the absence of complex and ΔA_s is the change in absorbance at the 560 nm in the presence of a given amount of complex. A representative plot of inhibition with increasing concentration of **1** is given in figure 1. Since the IC_{50} concentrations are proportional to the concentration of NBT, we calculated the apparent rate constants as $k_c = k[\text{NBT}]/IC_{50}$, where k is 5.94×10^4 $(\text{mol L}^{-1})^{-1}\,\text{s}^{-1}$ [37]. The determined IC_{50} and k_c values for the complexes are given in table 6. To ascertain the effectiveness of the reported complexes as functional SOD mimics, a comparison of the present obtained results with the literature data is shown in table 6. The catalytic activity of the natural enzyme is still unmatched [37]. The IC_{50} and k_c values obtained for the complexes here indicate that their SOD-like activities lie in the high activity of the spectrum exhibited by analogous copper(II) complexes [38–46]. The majority of the reported scavengers like our complexes exhibits k_c between 10^5 and 10^7 $(\text{mol L}^{-1})^{-1}\,\text{s}^{-1}$. A full overview of the possible reasons for the relative SOD-like activities of the many types of copper(II)

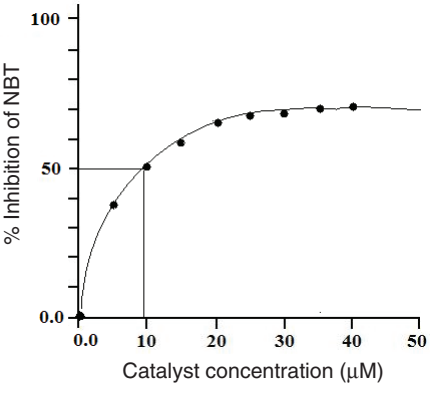

Figure 1. Plot of percentage of NBT inhibition reduction with an increase in the concentration of **1**.

complexes is out of the scope of this article. However, some specific remarks can be made. Thermodynamically competent $E_{1/2}$ for the concerned oxidation states of the metal center appears to be a necessary condition for catalysis. For example, investigation of the SOD mimetic activities of a series of copper(II) macrocyclic containing N_4 donor sets (similar to our complexes) shows that higher SOD-like activity is observed for complexes with $E_{1/2}$ values close to CuZnSOD [47]. In this case the $E_{1/2}$ value for the Cu(II)/Cu(I) couple was concluded to drive the SOD-like activity [41]. A series of macrocyclic copper(II) complexes exhibited appreciable SOD-like catalytic activities although their cyclic voltammetry measurements clearly demonstrated that the $E_{1/2}$ values of the Cu(II)/Cu(I) couple are not in the desired range [42]. Accordingly, they have been characterized as stoichiometric scavengers of $O_2^{\cdot-}$.

The ping-pong mechanism proposed for the dismutation of superoxide anion radical by both native SOD and copper(II) complexes is thought to involve redox cycling of copper(II) as follows:

$$Cu^{2+} + O_2^{\cdot-} \rightarrow Cu^{+} + O_2$$

$$Cu^{+} + O_2^{\cdot-} \rightarrow Cu^{2+} + O_2^{2-} \xrightarrow{H^+} Cu^{2+} + H_2O_2$$

To make a metal complex thermodynamically competent in the superoxide scavenging reaction, the redox potential of the metal center should fall in between the redox potentials of the two steps of the spontaneous dismutation process: the $O_2/O_2^{\cdot-}$ at -0.14 V *versus* NHE and the $O_2^{\cdot-}/H_2O_2 + 0.89$ V *versus* NHE at pH = 7 [31]. This requirement is fulfilled in the case of **1**–**5** as seen from the $E_{1/2}$ values in table 5. The position of the redox waves is governed by the nature of the counter-anion incorporated in the complex. The redox potential ($E_{1/2}$) values of the macrocyclic copper(II) complexes (table 5) are in the allowed range of an SOD mimic.

Table 6. Comparison of the superoxide dismutase biomimetic catalytic activities of **1–5** with known copper(II) macrocyclic complexes.

Complex	IC_{50} (mol L^{-1})	k_c (mol L^{-1})$^{-1}$ S^{-1}	Reference
1	$(08.85 \pm 0.15) \times 10^{-6}$	1.14×10^{6}	This work
2	$(17.50 \pm 0.81) \times 10^{-6}$	5.77×10^{5}	This work
3	$(05.50 \pm 0.19) \times 10^{-7}$	1.84×10^{7}	This work
4	$(38.50 \pm 1.03) \times 10^{-6}$	2.62×10^{5}	This work
5	$(39.50 \pm 1.10) \times 10^{-6}$	2.55×10^{5}	This work
native CuZnSOD	4.00×10^{-9}	2.52×10^{9}	[37]
$[Cu(TAAB)]^+$	1.44×10^{-7}	7.01×10^{7}	[39]
$[CuLH_2OCl]Cl\ H_2O$	1.3×10^{-5}	7.76×10^{5}	[40]
$L^2Cu_2(EtOH)_2$	$(1.42 \pm 0.13) \times 10^{-5}$	7.76×10^{5}	[41]
$L^2H_3Cu(EtOH)NO_3$	$(9.36 \pm 0.80) \times 10^{-5}$	1.07×10^{5}	[41]
$L^2H_3Cu(EtOH)Br$	$(2.19 \pm 0.50) \times 10^{-5}$	4.61×10^{5}	[41]
$L^2H_4CuCl_2(H_2O)_6$	$(4.36 \pm 0.69) \times 10^{-6}$	2.31×10^{6}	[41]
CuL^1	6.86×10^{-6}	1.47×10^{6}	[42]
CuL^2	18.84×10^{-6}	5.35×10^{5}	[42]
CuL^3	30.82×10^{-6}	3.27×10^{5}	[42]
CuL^4	13.94×10^{-6}	7.24×10^{5}	[42]
1	62.00×10^{-6}	1.62×10^{5}	[43]
2	26.00×10^{-6}	3.87×10^{5}	[43]

Complex details are as listed in table 1.

Although the square-planar complexes (**4** and **5**) possess redox potential values approaching square-pyramidal **2**, the latter exhibit greater reactivity. Approximately half of the IC_{50} concentration of **2** is enough to reach the 50% inhibition rate as compared with **4** and **5**. Thus the difference in reactivity of these chelates is not dependent only on the electrochemical character of copper(II), but the catalytic activity is governed by the geometry of Cu^{II} centers. Thus, a possible explanation for the lower SOD activity of the square planar complexes, **4** and **5**, as compared to the square-pyramidal **2** could be related to geometry. It has been previously reported that a strong equatorial ligand field opposes interaction of the complexed copper with $O_2^{\cdot-}$, disfavoring formation of the intermediate copper superoxide adduct [48]. A strong field disfavors reduction from copper(II) to copper(I) during the catalytic cycle. We suggest that coordination of the fifth ligand to copper(II) ion in the distorted square-pyramidal complex may reduce the strength of the equatorial field experienced by the copper(II) centers as compared to the square-planar complexes. Another important factor in the catalytic process is the ability of the five-coordinate complex to change its geometry as the geometry of copper in the CuSOD enzyme also changes from square-pyramidal [49]. This hypothesis finds support from Patel and co-workers, who reported that higher SOD activity of the five-coordinate copper(II) complexes is due to the presence of the fifth ligand in the axial position [50]. Interaction between the superoxide anion radical and copper(II) in the five-coordinate geometry is due to the strong axial bond which results in an increased catalytic activity [51].

3.7. *Catalase biomimetic catalytic activity*

Decomposition of hydrogen peroxide has been used as a model reaction for the investigation of the catalytic activity of various metal complexes and also as a catalase model, although the catalytic mechanism has not been thoroughly elucidated [52]. Decomposition of H_2O_2 to H_2O and O_2 is accelerated by many metal ions [53]. Especially, complexes of copper(II) with various ligands acting as catalysts have disagreements over mechanistic details, especially involving intermediate radicals or complexes.

Reaction of catalase models with H_2O_2 in pH = 7 medium rapidly leads to a new absorption at $\lambda_{max} = 385$ (figure 2). The reaction between H_2O_2 and these copper(II) catalase models was then monitored spectrophotometrically at $\lambda_{max} = 385\,nm$ by following the decrease in the absorbance with time. The absorbance–time data were introduced in the first-order equation (1):

$$\ln A_t = \ln A_0 - kt \tag{1}$$

where A_t is the absorbance of the undecayed intermediate adduct [catalyst–H_2O_2] at time t and k is the catalytic rate constant which was calculated from the slope of equation (1). The catalase biomimetic catalytic activity of **1**–**5** toward disproportionation of H_2O_2 was investigated by measuring the catalytic rate constant k_{obs} (table 5). The mechanism proposed for the disproportionation of H_2O_2 by both the native catalase and metal complexes is thought to involve redox cycling of metal ion as follows:

$$M^{n+} + H_2O_2 \rightarrow M^{(n-1)+} + HOO^{\cdot} + H^+, \tag{2}$$

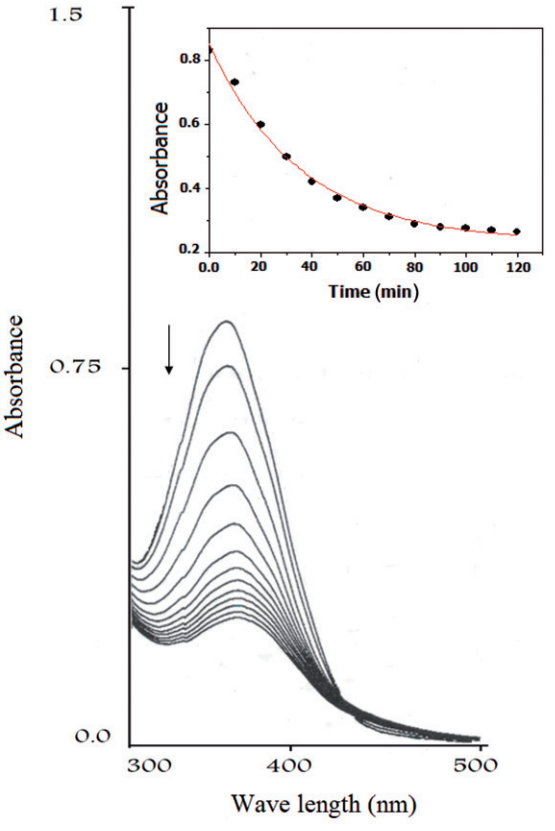

Figure 2. UV-Vis spectral changes recorded for reaction of **3** (1×10^{-3} mol L^{-1}) with H_2O_2 (10 mmol) at 296 K and at 385 nm. Inset shows the course of the absorption maximum at 385 nm with the time.

$$M^{(n-1)+} + HOO^{\cdot} + H^+ + H_2O_2 \rightarrow M^{n+} + 2H_2O + O_2. \quad (3)$$

The data in table 5 reveal that there is a correlation between electrochemical properties and catalase biomimetic catalytic capabilities of the copper(II) complexes. The redox potential ($E_{1/2}$) of these catalase models follows the order **4** > **5** > **2** > **1** > **3**, and the trend in catalytic efficiency almost follows the inverse of this order. This reflects that the balance between ease of reduction of copper(II) and subsequent reoxidation of copper(I) by the different interacted oxygen species during the catalytic cycle must be maintained for efficient catalysis to occur. This implies that a window of $E_{1/2}$ values exists wherein effective catalysis can take place. If the reduction potential is too negative, reduction to copper(I) is unattainable; on the other hand, if the reduction potential is too positive, the catalytic cycle would be short-circuited because once reduced to copper(I), the complexes would be unable to be easily reoxidized to copper(II). Reported models have been able to balance the requirements of the different oxidation states of the metal $M^{n+} \rightleftharpoons M^{(n-1)+}$ in performing their catalytic tasks.

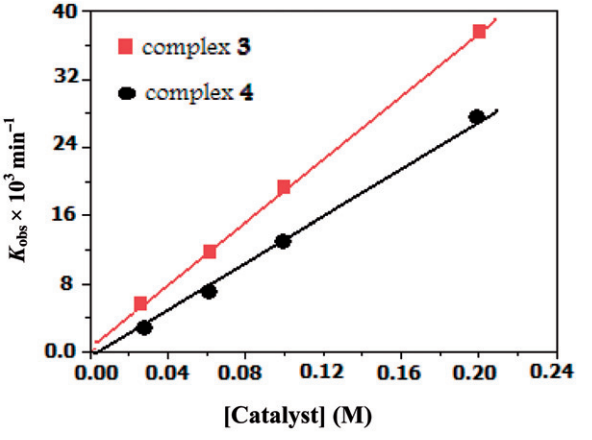

Figure 3. Plot of k_{obs} *vs.* catalyst concentration for the reaction between H_2O_2 and **3** and **4** at 296 K.

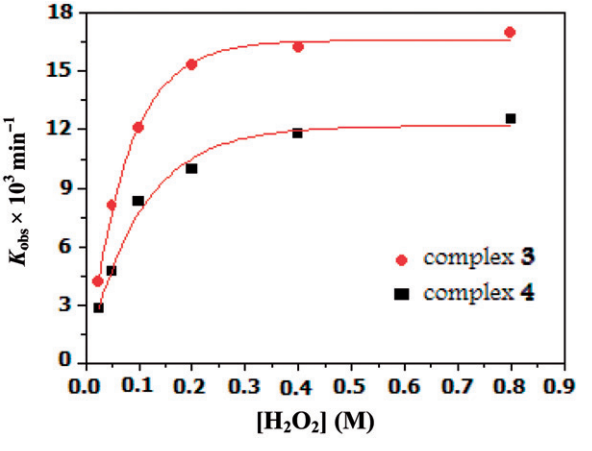

Figure 4. Plot of k_{obs} *vs.* H_2O_2 concentration for reaction of H_2O_2 with **3** and **4** at 296 K.

In order to define the reaction mechanism of the catalytic disproportionation of H_2O_2 by the reported catalase models, simple kinetics in various catalysts and H_2O_2 concentration conditions were investigated. While the initial concentration of H_2O_2 was held constant, the reaction was studied with variable amounts of catalyst (0.025–0.2 mol L^{-1}). Catalytic decomposition of H_2O_2 increased with increasing concentration of catalyst. The plots of k_{obs} against the amount of catalyst gave a linear relationship (figure 3), indicating that the reaction follows first-order kinetics with respect to catalyst concentration. As the lines in figure 3 pass through the origin, i.e., no intercept, there is no measurable rate of H_2O_2 decomposition in the absence of the catalyst.

Plots of k_{obs} against the amount of H_2O_2 are shown in figure 4, where the linearity at lower [H_2O_2] suggests first-order dependence, whereas at higher concentrations the reaction rate becomes independent of [H_2O_2]. This behavior indicates that catalytic decomposition of H_2O_2 follows Michaels–Menten kinetics.

A tentative reaction mechanism has been proposed utilizing the oxidative and reductive properties of H_2O_2 as reported elsewhere [54]. Native catalase catalyzes the disproportionation of H_2O_2 as shown in equation (4):

$$[LM]^{n+} + 2H_2O_2 \rightarrow [LM]^{n+} + 2H_2O + O_2. \quad (4)$$

At neutral pH, disproportionation of H_2O_2 by copper(II) complexes depends on concentration of $[LCu^{II}X]^+$ and H_2O_2 in solution according to rate equation (5):

$$-d[H_2O_2]/dt = k_{obs}[CuLX][H_2O_2]. \quad (5)$$

4. Conclusion

This article reports the synthesis and characterization of a series of copper(II) complexes of N_4 donor tetraazamacrocyclic ligand obtained by self-condensation of AMPC in the presence of copper(II). The physical properties and structures of these macrocyclic complexes depend on the nature of the counter anion. Square-pyramidal five-coordinate (nitrato and halogeno) and four-coordinate square-planar (perchlorate and acetate) stereochemistries have been proposed based on the positions of bands in the electronic spectra and the magnetic measurements (μ_{eff} and ESR). ESR studies revealed the similarity of copper(II) environment in the five-coordinate, nitrato, with halogeno complexes. The antioxidant biomimetic catalytic activity studies revealed that these chelates are functional models of both SOD and catalase enzymes. There is a correlation between the observed redox properties and the SOD– and catalase biomimetic catalytic capabilities of the copper(II) complexes (the higher SOD/catalase-like activities are observed for the complex with $E_{1/2}$ close to CuZnSOD (+300 mV). The four-coordinate complexes have lower antioxidant catalytic activity as compared to the five-coordinate species. This behavior can be related to the strong equatorial field of the square-planar arrangement which does not favor attack of the ROS, e.g., $O_2^{\cdot-}$, $HO_2^{\cdot}$, or H_2O_2, to accessible apical sites during the disproportionation catalytic cycle.

References

[1] R.R. Crichton. *Biological Inorganic Chemistry*, 1st Edn, Elsevier, Amsterdam (2008).
[2] B. Chance, H. Sies, A. Boveris. *Physiological Rev.*, **59**, 527 (1979).
[3] A. Boveris. *Methods Enzymol.*, **105**, 429 (1984).
[4] J.F. Turrens, A. Alexandre, A.L. Lehninger. *Arch. Biochem. Biophys.*, **237**, 408 (1985).
[5] M.F. Beal, N. Howell, I. Bodis-Wollner. *Mitochondria and Free Radicals in Neurodegenerative Diseases*, 1st Edn, Wiley-Liss, New York (1997).
[6] J. Sessler, S.R. Doctrow, T.J. McMurry, S.J. Lippard. *Medicinal Inorganic Chemistry*, 1st Edn, p. 903, ACS Symposium Series, New York (2005).
[7] (a) M.F. Beal. *Curr. Opin. Neurobiol.*, **6**, 661 (1996); (b) A. Rotig, P. Ddelonlay, D. Chretien, F. Foury, M. Koenig, D. Sidi, A. Munnich, P. Rustin. *Nature Genetics*, **17**, 215 (1997); (c) K.B. Beckman, B.N. Ames. *Physiol. Rev.*, **78**, 547 (1998); (d) S.I. Choi, W.K. Ju, E.K. Choi, J. Kim, H.Z. Lea, R.I. Carp, H.M. Wisniewski, Y.S. Kim. *Acta Neuropath.* (Berl.), **96**, 279 (1998); (e) A.H.V. Schapira. *Biochim. Biophys. Acta*, **1366**, 225 (1998); (f) M.A. Smith, L.M. Sayre, V.E. Anderson, P.L. Harris, M.F. Beal, N. Kowall, G.J. Perry. *Histochem. Cytochem.*, **46**, 731 (1998); (g) C. Behl. *Prog. Neurobiol.*, **57**, 301 (1999); (h) A.R White, X. Huang, M.F. Jobling, C.J. Barrow, K. Beyreuther, C.L. Masters, A.I. Bush, R Cappai. *J. Neurochem.*, **76**, 1509 (2001); (i) C. Jung, C.M. Higgins, Z. Xu, *J. Neurochem.*, **83**, 535 (2002).

[8] K. Yasui, A. Baba. *Inflamm. Res.*, **55**, 359 (2006).
[9] (a) D. Salvemini, T.M. Doyle, S. Cuzzocrea. *Biochem. Soc. Trans.*, **34**, 965 (2006); (b) B.J. Day. *Antioxidant Redox Signal*, **10**, 355 (2008); (c) S. Melov, S.R. Docttow, J.A. Schneider, J. Haberson, M. Patel, I.E. Coskun, K. Huffman, D.C. Wallace, B. Malfroy. *J. Neurosci.*, **21**, 8348 (2001).
[10] R.J. Ferrante, S.E. Browne, R.T. Matthews, N.W. Kowall, R.H. Brown. *J. Ann. Neurol.*, **42**, 644 (1997).
[11] A. Hirano, M. Kobayashi, S. Sasaki, T. Kato, S. Matsumoto, Z. Shiozawa, T. Komori, A. Ikemoto, T. Umahara. *Neurosci. Lett.*, **179**, 149 (1994).
[12] K. Baker, C.B. Marcus, K. Huffman, H. Kruk, B. Malfroy, S.R. Doctrow. *J. Pharmacol. Exp. Ther.*, **284**, 215 (1998).
[13] V. Lanaza, G. Vecchio. *J. Inorg. Biochem.*, **103**, 381 (2009).
[14] A. Gartner, U. Weser. In *Topics in Current Chemistry*, F. Vogle, E. Weber (Eds), Vol. 132, p. 1, Springer, Berlin (1986).
[15] D. Darr, K.A. Zarilla, I. Fridovich. *Arch. Biochem. Biophys.*, **258**, 351 (1987).
[16] D.P. Riley. *Chem. Rev.*, **99**, 2573 (1999).
[17] E. Bienvenue, S. Choua, M.A. Lobo-Recio, C. Marzin, P. Pacheco, P. Seta, G. Tarrago. *J. Inorg. Biochem.*, **57**, 157 (1995).
[18] L.F. Lindoy. *The Chemistry of Macrocyclic Ligands Complexes*, Cambridge University Press, Cambridge, UK (1989).
[19] J. Haufel, E. Beitmaier. *Angew. Chem.*, **13**, 604 (1974).
[20] A.M. Ramadan, T.I. El-Emary. *Trans. Met. Chem.*, **23**, 491 (1998).
[21] S. Chandra, S.D. Sharma. *Trans. Met. Chem.*, **27**, 73 (2002).
[22] C. Lodeiro, R. Basitida, E. Bertolo, A. Macias, R. Rodriguez. *Trans. Met. Chem.*, **28**, 388 (2003).
[23] P.M. Reddy, A.V.S.S. Prasad, K. Shanker, V. Ravinder. *Spectrochim. Acta A*, **68**, 1000 (2007).
[24] G.A. Nelson, D.H. Bush. *J. Am. Chem. Soc.*, **86**, 4834 (1964).
[25] S. Brawner, K.B. Mertes. *J. Inorg. Nucl. Chem.*, **41**, 764 (1979).
[26] K. Nakamoto. *Infrared and Raman Spectra of Inorganic and Coordination Compounds*, Wiley, New York (1986).
[27] A.M. Ramadan, M.M. El-Naggar. *J. Inorg. Biochem.*, **63**, 143 (1996).
[28] A.B.P. Lever. *Inorganic Electronic Spectroscopy*, Elsevier, Amsterdam (1970).
[29] (a) B.N. Figgis, J. Lewis. *Prog. Inorg. Chem.*, **6**, 37 (1964); (b) R.L. Dutta, A. Syamal, *Elements of Magnetochemistry,* 2nd Edn, Affiliated East-West Press, Delhi (2007).
[30] K. Kivelson, R. Neiman. *J. Chem. Phys.*, **35**, 149 (1961).
[31] J. Petlicki, T.G.M. van de Ven. *J. Chem. Soc., Faraday Trans.*, **94**, 2763 (1998).
[32] D. Salvemini, D.P. Riley, S. Cuzzocrea. *Nature Rev. Drug Discov.*, **1**, 367 (2002).
[33] J.R.J. Sorenson. *Prog. Med. Chem.*, **26**, 437 (1989).
[34] (a) X. Liang, P.J. Sadler. *Chem. Soc. Rev.*, **33**, 246 (2004); (b) F. Marques, L.Gano, M.P. Campello, S. Lacerda, I. Santos, L.M. Lima, J. Costa P. Antunes, R. Delgado. *J. Inorg. Biochem.*, **100**, 270 (2006); (c) F. Marques, K.P. Guerra, L. Gano, M.P. Campello, L.M. Lima, J. Costa P. Antunes, R. Delgado, I. Santos. *J. Inorg. Biochem.*, **9**, 859 (2004).
[35] (a) D.P. Riley. *Chem. Rev.*, **99**, 2573 (1999); (b) H.L. Zhu, Q.W. Hang, J. Zhao, C.Y. Duan, W.X. Tang. *Trans. Met. Chem.*, **24**, 131 (1999).
[36] B.H.J. Beilski, H.W. Richter. *J. Am. Chem. Soc.*, **99**, 3019 (1977).
[37] D. Klug, I. Frodovich, J. Rabani. *J. Am. Chem. Soc.*, **95**, 2786 (1973).
[38] Z. Liao, W. Liu, J. Liu, Y. Jiang, J. Shi, C. Liu. *J. Inorg. Biochem.*, **55**, 165 (1994).
[39] Z. Durackova, J. Labuda. *J. Inorg. Biochem.*, **58**, 297 (1995).
[40] E. Bienvenue, S. Choua, M.A. Lobo-Recio, C. Marzin, P. Pacheco, P. Seta, G. Tarrago. *J. Inorg Biochem.*, **57**, 157 (1995).
[41] Z. Durackova, M.A. Mendiola, M.T. Sevilla, A. Valent. *Bioelectrochem. Bioenerg.*, **48**, 109 (1999).
[42] A.S. Fernandes, J. Gaspar, M.F. Cabral, C. Caneiras, R. Guedes, J. Rueff, M. Castro, J. Costa, N.G. Oliveira. *J. Inorg. Biochem.*, **101**, 849 (2007).
[43] D. Li, S. Li, D. Yang, J. Yu, J. Huang, Y. Li, W. Tang. *Inorg. Chem.*, **42**, 6071 (2003).
[44] V. Lanza, G. Vecchio. *J. Inorg. Biochem.*, **103**, 381 (2009).
[45] A. Abuhijleh, J. Khalaf. *Eur. J. Med. Chem.*, **45**, 3811 (2010).
[46] A. Abuhijleh. *Inorg. Chem. Commun.*, **14**, 759 (2011).
[47] D.T. Sawyer, J.S. Valentine. *Acc. Chem. Res.*, **14**, 393 (1981); (b) G. Czapski, S. Goldstein. *Free Rad. Res. Commun.*, **4**, 225 (1988).
[48] R.P. Bonomo, E. Conte, R. Marcelli, A.M. Sontoro, G.J. Tabi. *J. Inorg. Biochem.*, **53**, 172 (1994).
[49] (a) S.J. Lipard, A.R. Burger, K. Ugurbil, J.S. Valentine, W. Pantaliano. In *Bioinorganic Chemistry*, K.N. Raymond (Ed.), American Chemical Society, Washington, DC (1977); (b) J.S. Richardson, D.C. Richardson, J.A. Trainer, E.D. Galtzoff. *Nature*, **306**, 284 (1986).
[50] R.N. Patel, N. Singh, K.K. Shukla, V.L.N. Gundla, U.K. Chauhan. *J. Inorg. Biochem.*, **99**, 651 (2005); (b) R.N. Patel, N. Singh, K.K. Shukla, U.K. Chauhan, J.N. Gutierrez, A. Castineiras. *Inorg. Chim. Acta*, **357**, 2469 (2004).

[51] J.P. Collman, T.R. Halbert, K.S. Suslick. In *Metal Ion in Activation of Dioxygen*, T.G. Spiro (Ed.), Wiley, New York (1980).
[52] (a) M. Kaneko, E. Tsuchida. *J. Polym. Sci. Makromol. Rev.*, **16**, 397 (1981); (b) E. Tsuchida, H. Nishide. *Adv Polym. Sci.*, **24**, 1 (1977); (c) M. Nath, K. Cheema, J. Cheema. *Ind. J. Chem.*, **32A**, 108 (1993); (d) J. Gao, A.E. Martell, J.H. Reibenspies. *Inorg. Chim. Acta*, **346**, 32 (2003); (e) M. Devereux, D.O. Shea, A. Kellett, M. McCann, M. Walsh, D. Egan, C. Deegan, K. Kedziora, G. Rosair, H. Muller-Bunz. *J. Inorg. Biochem.*, **101**, 881 (2007); (f) V. Lanza, G. Vecchio. *J. Inorg. Biochem.*, **103**, 381 (2009); (g) A.E.O. Fisher, S.C. Maxwell, D.P. Naughton. *Inorg. Chem. Commun.*, **6**, 1205 (2003).
[53] (a) F. Haber, J. Wiss. *Proc. R. Soc. London, Ser. A*, **147**, 332 (1934); (b) W.G. Barb, J.H. Baxendale, P. George, K.R. Hargrave. *Trans. Faraday Soc.*, **47**, 462 (1951); (c) M.L. Kremer, G. Stein. *Trans. Faraday Soc.*, **55**, 959 (1959); (d) A. Glasner. *J. Chem. Soc.*, **904**, 2464 (1959); (e) M.L. Kremer. *Int. J. Chem. Kinet.*, **17**, 1299 (1985).
[54] R.N. Ram. *Kinet. Catal.*, **25**, 700 (1984).